Research Square

Preprints are preliminary reports that have not undergone peer review.
They should not be considered conclusive, used to inform clinical practice,
or referenced by the media as validated information.

Synthesis of a calcium silicate-carbonate at 122 GPa reveals a missing link in deep-mantle chemistry of silicates and carbonates

Georgios Aprilis

georgios.aprilis@esrf.fr

ESRF, The European Synchrotron, 71 Avenue des Martyrs, CS40220, 38043 Grenoble Cedex 9, France
https://orcid.org/0000-0002-0020-9125

Apostolos Pantousas
European Synchrotron Radiation Facility https://orcid.org/0009-0000-9020-4039

Alena Aslandukova
Goethe University Frankfurt

Ilya Kupenko
Europian Synchrotron Radiation Facility

Xiang Li
European Synchrotron Radiation Facility https://orcid.org/0000-0003-3259-1784

Susanne Müller
European Synchrotron Radiation Facility

Michael Hanfland
European Synchrotron Radiation Facility

Leonid Dubrovinsky
Bayerisches Geoinstitut https://orcid.org/0000-0002-3717-7585

Anna Pakhomova
European Synchrotron Radiation Facility

Article

Keywords:

Posted Date: December 9th, 2025

DOI: https://doi.org/10.21203/rs.3.rs-8308717/v1

License: This work is licensed under a Creative Commons Attribution 4.0 International License.
Read Full License

Additional Declarations: There is **NO** Competing Interest.

Version of Record: A version of this preprint was published at Nature Communications on September 4th, 2026. See the published version at https://doi.org/10.1038/s41467-026-77204-w.

Synthesis of a calcium silicate-carbonate at 122 GPa reveals a missing link in deep-mantle chemistry of silicates and carbonates

*Georgios Aprilis[1], Apostolos Pantousas[1, 2], Alena Aslandukova[3], Ilya Kupenko[1], Xiang Li[1], Susanne Müller[1, 4], Michael Hanfland[1], Leonid Dubrovinsky[2] and *Anna Pakhomova[1]

[1]European Synchrotron Radiation Facility, Grenoble, France

[2]University of Bayreuth, Bayreuth, Germany

[3]Goethe University Frankfurt, Frankfurt am Main, Germany

[4]University of Münster, Münster, Germany

*corresponding author

Abstract

Interactions between carbonates and silicates play a central role in many industrial and planetary processes. Although current knowledge is largely limited to silicate–carbonate exchange mechanisms, high-pressure compounds incorporating both carbonate and silicate units have long been anticipated. Here we report the synthesis of the high-pressure silicate–carbonate $CaSiC_2O_7$ at 122(2) GPa and 2800(200) K. $CaSiC_2O_7$ is based on the framework of vertex-sharing SiO_6 octahedra and CO_4 tetrahedra. *Ab initio* calculations are consistent with the experimental results and indicate dynamical and mechanical stability of this phase over a wide pressure range. These findings reveal an additional pathway for carbonate–silicate interaction in carbonate-rich deep-mantle environments. $CaSiC_2O_7$ has a density lower than that of major mantle minerals and exhibits comparatively low acoustic velocities, suggesting that silicate-carbonates may contribute to seismic anomalies near the core–mantle boundary.

Introduction

Carbonates and silicates are fundamental to both chemistry and planetary science. They are important technological materials with a wide range of applications, including cement production (Scrivener et al. 2018), catalysis (Yang et al. 2025), water treatment (Bhatnagar and Sillanpää 2010) among others. As geomaterials, silicates are the most abundant minerals in the Earth's crust and mantle thereby defining its structure and evolution. In turn, carbonates play a key role in regulating the Earth's climate and habitability, as they are responsible for long-term hosting and recycling of the CO_2 through subduction (Dasgupta and Hirschmann 2010). In addition, both silicates and carbonates are often discussed as contributors to the Earth's seismic anomalies (Lebedev et al. 2002; Wentzcovitch et al. 2006; Wang et al. 2024; Zhang et al. 2025).

Despite the fact that carbon and silicon are both group IV elements, their oxides reveal remarkably different bond characteristics. At ambient conditions, the crystal chemistry of carbonates is driven by sp^2 hybridization of carbon atomic orbitals which allows the formation of $[CO_3]^{2-}$ groups with triangular planar geometry. In contrast, silicon adopts sp^3 hybridization in most of the silicates, forming four directional bonds in a tetrahedral geometry $[SiO_4]^{4-}$. Interaction between carbonates and silicates draws long-lasting attention, driven by interest in CO_2 sequestration in silicate-based cements (Kunther et al. 2017; Seifu et al. 2023), silicate-carbonate global cycle (Penman et al. 2020) and fate of subducting carbonates upon contact with silicate mantle (Biellmann et al. 1993; Seto et al. 2008; Lv et al. 2021). In industrial and geological processes, silicate-carbonate exchange reactions (primarily involving $(Ca,Mg)SiO_3$ and $(Ca,Mg)CO_3$) are dominant and silicate-carbonate compounds containing both carbon and silicon are quite rare. To the best of our knowledge, the only class of silicate-carbonates are minerals (Lazic et al. 2011; Marincea et al. 2013) based upon CO_3 and SiO_4 polyhedra and usually formed at elevated temperatures (up to ~1300 K) and moderate pressures (up to ~1 GPa).

High-pressure is a powerful tool that allows the formation of new phases with properties and stoichiometries unexpected from the viewpoint of conventional solid-state chemistry (Grochala et al. 2007). Pressure-induced densification typically increases atomic coordination (often given as Roman numbers). This trend is well-established for silicates where silicon transitions from four-fold (SiO_4, or Si[IV]) towards six-fold (SiO_6, or Si[VI]) coordination (Prewitt and Downs 1998; Hazen et al. 2018; Krivovichev 2021), with the occasional formation of transient

five-fold SiO_5 (Si[V]) state (Finkelstein et al. 2015; Hu et al. 2017; Pakhomova et al. 2017, 2020). Similarly, a change from sp^2- to sp^3-configuration of carbon (Oganov et al. 2013; Gao et al. 2022) drives high-pressure chemistry of carbonates (Boulard et al. 2015; Merlini et al. 2020; Cerantola et al. 2023) and results in the formation of CO_4 tetrahedra (C[IV]). This tendency reduces the chemical difference between carbonates and silicates as shown experimentally (Santoro et al. 2011) and theoretically (Zhou 2014, 2014) for $Si_xC_{1-x}O_2$ compound at 18-26 GPa and 600 – 980 K. Although silicate-carbonate compounds containing both C[IV] and Si[VI] were long predicted to exist under high pressure (Oganov et al. 2013), they have never been observed experimentally.

Herein, we report on the synthesis of $CaSi^{[VI]}C^{[IV]}{}_2O_7$ in a laser-heated diamond anvil cell. *In situ* synchrotron-based single-crystal X-Ray diffraction of a polycrystalline sample was employed to solve and refine its structure at 122 GPa. *Ab initio* density functional theory has been employed to extend the experimental observation, particularly to derive its equation of state and elastic constants. Synthesis of the $CaSiC_2O_7$ marks an important benchmark in the high-pressure inorganic chemistry and geochemistry. It is the first experimentally observed high-pressure silicate-carbonate built upon CO_4 tetrahedra and SiO_6 octahedra as well as the first sp^3-pyrocarbonate possessing $[C_2O_7]^{6-}$ units. Besides, our results demonstrate a novel pathway of interactions between carbonates and silicates at conditions of the lowermost lower mantle and suggest silicate-carbonates as possible contributors to its seismic anomalies.

Results

Experimentally derived crystal structure of the $CaSiC_2O_7$

The silicate-carbonate $CaSi^{[VI]}C^{[IV]}{}_2O_7$ was synthesized upon reaction between $CaSiO_3$ and $CaCO_3$ at 122(2) GPa and 2800(200) K in a laser-heated diamond anvil cell ($Fe_{0.945}O$ was used as laser light absorber, see *Methods* for details). The $CaSiC_2O_7$ compound crystalizes in the orthorhombic space group *Cmcm (#63)* with a = 4.4750(2) Å, b = 6.4691(8) Å, c = 9.013(3) Å, V = 260.9193(16) Å^3. The asymmetric unit of $CaSiC_2O_7$ contains one calcium, one carbon, one silicon, and three oxygen atoms (Figure 1). Calcium cations are 12-fold coordinated with formation of cuboctahedra, silicon atoms are octahedrally coordinated and carbon atoms are in tetrahedral coordination (Figure 2). The Ca-O bond distances slightly vary in the range of 2.221(5) to 2.317(6) Å with an average of 2.26 Å (Figure 2c). The SiO_6 octahedra also possess a geometry close to a regular one. Two epical bonds Si-O2 and four equatorial bonds Si-O3 are of 1.627(4) Å and 1.635(4) Å, respectively, while O2-Si-O3 and O3-Si-O3 angles are of

88.53(18)° and 90.4(4)° (Figure 2b). The CO_4 tetrahedra reveal a higher level of distortion. C-O bond distances vary from 1.295(9) to 1.404(8) Å with an average of 1.329 Å (Figure 2a) while the tetrahedral angles O-C-O are in the range of 106.4(5) – 112.6(5)°. CO_4 tetrahedra link through common O1 vertices with formation of $[C_2O_7]^{6-}$ dimers. SiO_6 octahedra are isolated from each other and share with CO_4 tetrahedra common O2 and O3 vertices with the formation of the three-dimensional framework that hosts Ca atoms in its voids. It is also noteworthy that layers of Ca and O atoms are forming cubic close-packing arrangement where the C and Si atoms are filling tetrahedral and octahedral voids, respectively (Figure S1).

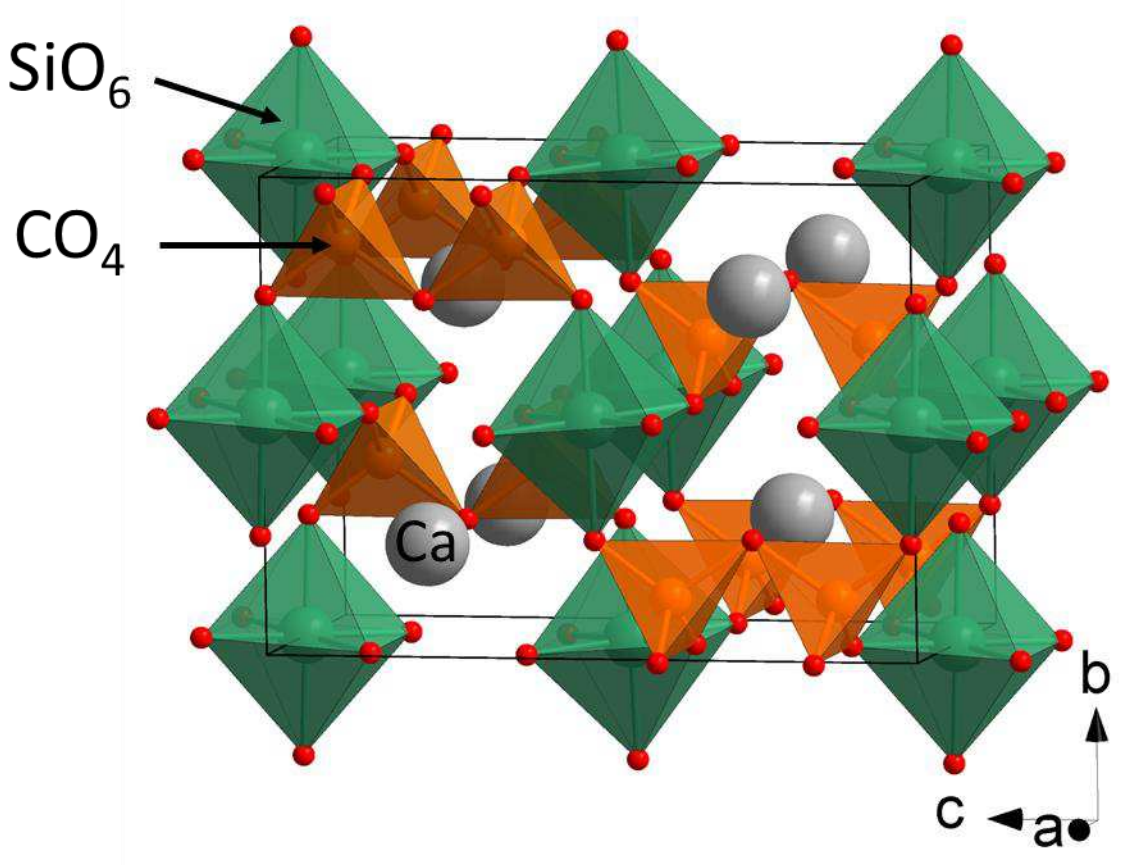


Figure 1. Polyhedral model of the crystal structure of $CaSiC_2O_7$ at 122 GPa obtained from single crystal X-Ray diffraction. CO_4 and SiO_6 polyhedra are given in orange and green, respectively. Ca and O atoms are given as grey and red spheres, respectively. The black lines outline the unit cell.

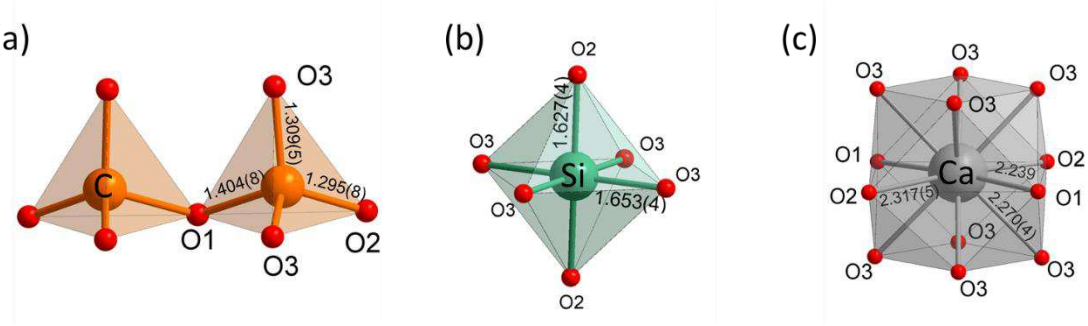


Figure 2. Structural units of the $CaSiC_2O_7$. (a) C_2O_7 dimer composed of two CO_4 tetrahedra; (b) SiO_6 octahedron; (c) CaO_{12} cuboctahedron. The oxygen atoms are given as red spheres.

The topology of $CaSiC_2O_7$ framework resembles the one of sodium trisilicate, $Na_2Si_2^{[VI]}Si_4^{[IV]}O_{14}$ (a = 8.922(2) Å, b = 4.8490(5) Å, c = 11.567(1) Å, β = 102.64(1)°, space group $C2/c$, Figure S2) (Fleet and Henderson 1995). The sodium trisilicate belongs to the group of high-pressure framework silicates with mixed 4- and 6-fold coordination of silicon (Hazen et al. 1996). Synthesized at pressures >4 GPa, these frameworks feature relatively dense arrangements of SiO_4 tetrahedra and SiO_6 octahedra and contain large sites suitable for alkali or alkaline-earth cations. Earlier, Oganov et al. (Oganov et al. 2013) proposed that these structures can be adapted by high-pressure silicate-carbonates (Fleet and Henderson 1995; Hazen et al. 1996). Herein we demonstrate for the first time that indeed at megabar pressures sp^3 carbon can substitute silicon in the tetrahedral site with the formation of a framework based on CO_4 and SiO_6 polyhedra.

Ab initio calculations for the $CaSiC_2O_7$.

The phase synthesised in this work has never been predicted. To assess whether the experimentally observed $CaSiC_2O_7$ phase can be reproduced theoretically, we have performed *ab initio* simulations (See *Methods*). Full structural relaxation at experimental unit cell volume results in an excellent agreement between measured and calculated unit-cell parameters, atomic coordinates and interatomic distances (Table S1). Harmonic phonon dispersion calculations reveal that the novel $CaSiC_2O_7$ is dynamically stable both at the synthesis pressure of 122 GPa and at 1 bar (Figure S3). The pressure dependence of the theoretical values of the unit cell volume of $CaSiC_2O_7$ can be described by the third-order Birch-Murnaghan equation of state with the parameters V_0 = 377.5(2) Å^3, K_0 = 151.2(9) GPa and K' = 4.41(2) (Figure 3).

The elastic constants (C_{ij}) of $CaSiC_2O_7$, calculated at 0 K for both at 122 GPa (Table S2) and at ambient pressures (Table S3), indicate that the phase is mechanically stable under these conditions, according to the Born stability criteria for orthorhombic systems (Text S1, Mouhat and Coudert 2014). The bulk and shear moduli were derived from the elastic tensor by the Voigt and Reuss approach (Text S2, Reuss 1929). As expected, the bulk modulus K = 155 GPa calculated from the elastic constants at 1 bar is consistent with the value K_0 = 151.2(9) GPa obtained from the equation-of-state fit, confirming the internal consistency of the calculations.

The calculated electronic density of states shows that $CaSiC_2O_7$ is a wide-bandgap semiconductor with a band gap (E_g) of 5.6 eV at 122 GPa (Figure S4).

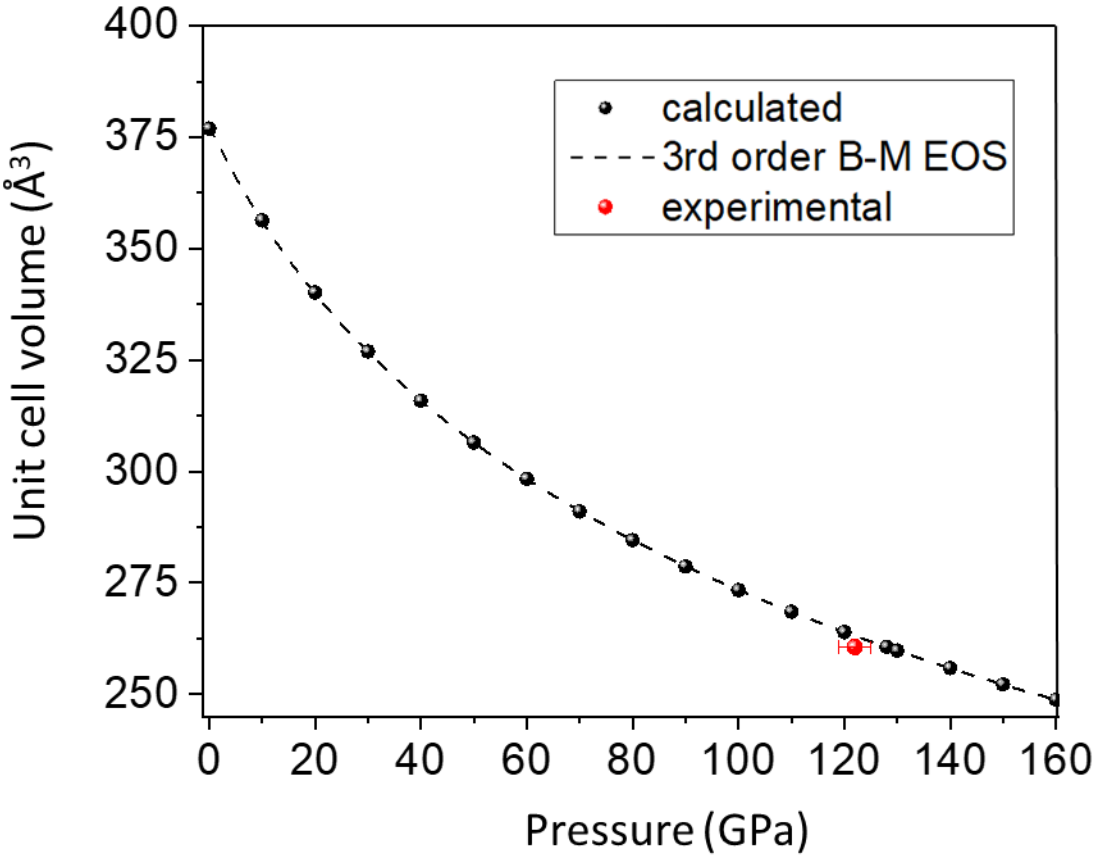


Figure 3. The pressure dependence of the $CaSiC_2O_7$ unit cell volume. Red solid circle represents experimental data, while black solid circles are values from the calculations. The black dashed line shows the fit of the calculated pressure-volume data using the third-order Birch-Murnaghan equation of state (V_0 = 377.5(2) Å^3, K_0 = 151.2(9) GPa and K' = 4.41(2)).

Discussion

New insight into high-pressure chemistry of carbonates-silicates

The current study pioneers to demonstrate the synthesis of the calcium silicate-carbonate, $CaSi^{[VI]}C^{[IV]}{}_2O_7$, based on CO_4 and SiO_6 units. Previously, about 50 silicate-carbonates were known at ambient conditions, with three being from the CaO-SiO_2-CO_2 system: spurrite, $Ca_5[SiO_4]_2(CO_3)$ (Grice 2005), tilleyite, $Ca_5[Si_2O_7](CO_3)_2$ (Larsen and Dunham 1933), and galuskinite, $Ca_7(SiO_4)_3(CO_3)$ (Lazic et al. 2011). While being based on CO_3 triangles and SiO_4 tetrahedra at ambient conditions, these compounds were proposed as possible precursors for high-pressure silicate-carbonates hosting C[IV] and/or Si[VI]. However, spurrite, $Ca_5[SiO_4]_2(CO_3)$, and tilleyite, $Ca_5[Si_2O_7](CO_3)_2$, were found to decompose into their component silicates and carbonates at pressures below 4 GPa at ~1300 K (Liu and Lin 1995). Recent studies at elevated temperatures demonstrated phase stability of spurrite up to 27 GPa and 700 K, with no phase transitions being observed (Santamaria-Perez et al. 2018). Tilleyite was also found to persist up to 7 GPa and 675 K, while at higher pressures it transformed to post-tilleyite phase containing again CO_3 and SiO_4 units (Santamaria-Perez et al. 2019). *Ab initio* calculations have also suggested the stability of these calcium silicate-carbonates minerals up to 25-35 GPa (Gao et al. 2015). The presence of rigid carbonate units was proposed to enhance stability of SiO_4 tetrahedra and to prevent their transition to SiO_6 octahedra (Santamaria-Perez et al. 2018). Our study demonstrates that these transitions can be induced by considerably higher pressures and temperatures. The discovered here $CaSi^{[VI]}C^{[IV]}{}_2O_7$ phase adapts the structure and stoichiometry of sodium trisilicate, $Na_2Si_2{}^{[VI]}Si_4{}^{[IV]}O_{14}$, thus hinting that other high-pressure framework silicates with mixed 4- and 6-fold coordination of silicon (Hazen et al. 1996) are promising isomorphs for silicate-carbonates.

Synthesized in this work $CaSiC_2O_7$ is the first example of a sp^3-pyrocarbonate hosting $[C_2O_7]$ units (Figure 2a). Our work broadens the known structural diversity of carbonates at high pressures and strengthens the connection between the crystal chemistry of high-pressure sp^3-carbonates and low-pressure tetrahedral silicates. Typically, structural diversity of C[IV] carbonates was considered more limited in contrast to Si[IV] silicates, due to smaller flexibility of inter-tetrahedral C-O-C angles in comparison to Si-O-Si angles (Oganov et al. 2008, 2013). However, recent advancement in carbonates chemistry allowed to experimentally discover nesocarbonates with isolated CO_4 tetrahedra (Me_2CO_4, Me = Ca, Sr) (Spahr et al. 2021; Binck et al. 2022), carbonates based on four-membered linear groups ($Me_4C_4O_{13}$, Me = Mg/Fe)

(Merlini et al. 2015; Cerantola et al. 2017; Chariton 2020) and four-membered pyramidal groups (MeC_2O_5, Me = Ca, Fe, Mn, Cd) (Chariton 2020; König et al. 2022; Wang et al. 2024; Kovalev et al. 2025), inocarbonates with infinite chains of vertice-sharing CO_4 tetrahedra ($CaCO_3$) (Ono et al. 2007; Lobanov et al. 2017), cyclocarbonates based on three-membered rings ($Me_3C_3O_9$, Me = Fe, Mg, Ca) (Boulard et al. 2011, 2015; Merlini et al. 2017; Chariton et al. 2020), and a tectocarbonate with three-dimensional connectivity of tetrahedra (CaC_2O_5) (Pantousas et al. 2025). Even greater structural diversity of carbonates is proposed on the base of theoretical calculations (Yao 2018; Wang et al. 2024), highlighting the need of further experiments to explore the complex chemistry of high-pressure sp^3-carbonates.

Implications for the deep carbon storage

The findings reported here in the geologically relevant system $CaCO_3$ – $CaSiO_3$ – FeO have several implications to the mineralogy and elasticity of Earth's lowermost mantle. Firstly, the discovery of $CaSiC_2O_7$ reveals a new class of carbon hosts in Earth's deep interior. Carbonates, predominantly calcite ($CaCO_3$) and dolomite ($Ca,Mg(CO_3)$), carry the inorganic carbon into the deeps via subduction and interact with the minerals of the average mantle upon the descend. Previous high-pressure-high-temperature studies within the (Ca,Mg,Fe)-Si-C-O system demonstrated that plethora of phases can be formed depending on the phase assemblages and experimental conditions, including polymorphs of $CaCO_3$, $MgCO_3$, $CaSiO_3$, $MgSiO_3$, Fe_3C, FeO, CaO, SiO_2, Fe_7C_3, C, MgO, CO_2 (Supplementary Table S4). These observations allowed to propose melting (Dasgupta and Hirschmann 2010), decarbonation (Seto et al. 2008; Kakizawa et al. 2015; Drewitt et al. 2019), silicate-carbonate chemical exchange (Biellmann et al. 1993; Lv et al. 2021; Davis et al. 2024), redox freezing with diamond or carbide formation (Arima et al. 2002; Seto et al. 2008; Rohrbach and Schmidt 2011; Dorfman et al. 2018; Zhu et al. 2019), as potential mechanisms that govern the fate of carbonates in the Earth's deeps. We pioneer to demonstrate a novel scenario of interaction between carbonates and silicates at the pressure and temperature conditions of the lowermost lower mantle, with the formation of silicate-carbonate compounds that host both carbon and silicon (Figure 4). In the light of the ongoing discussions on the redox heterogeneity of the lower mantle (Frost and Myhill 2016; Gu et al. 2016; Kaminsky 2020), presence of carbonates and silicate-carbonates can be envisioned in its locally oxidized domains, that are thought to arise from subducted crustal materials (Hirschmann 2023), Fe^{3+} disproportionation reactions (Frost et al. 2004; Frost and McCammon 2008), or core–mantle exchange processes (Frost et al. 2008). Persistence of oxidized forms of carbon under these conditions is supported by the occurrence of carbonates

as inclusions in deep diamonds (Korsakov and Hermann 2006; Kaminsky 2012; Agrosì et al. 2019) as well as by experimental evidence of calcium carbonate formation from reactions between calcium silicate and iron carbides (Davis et al. 2024). Importantly, calcium carbonates were also proposed to be less sensitive than (Mg,Fe)CO_3 to redox breakdown throughout the lower mantle (Dorfman et al. 2018). These observations advocate for the possible presence of carbonates in the deep mantle and their availability for interactions with the abundant lower mantle silicates.

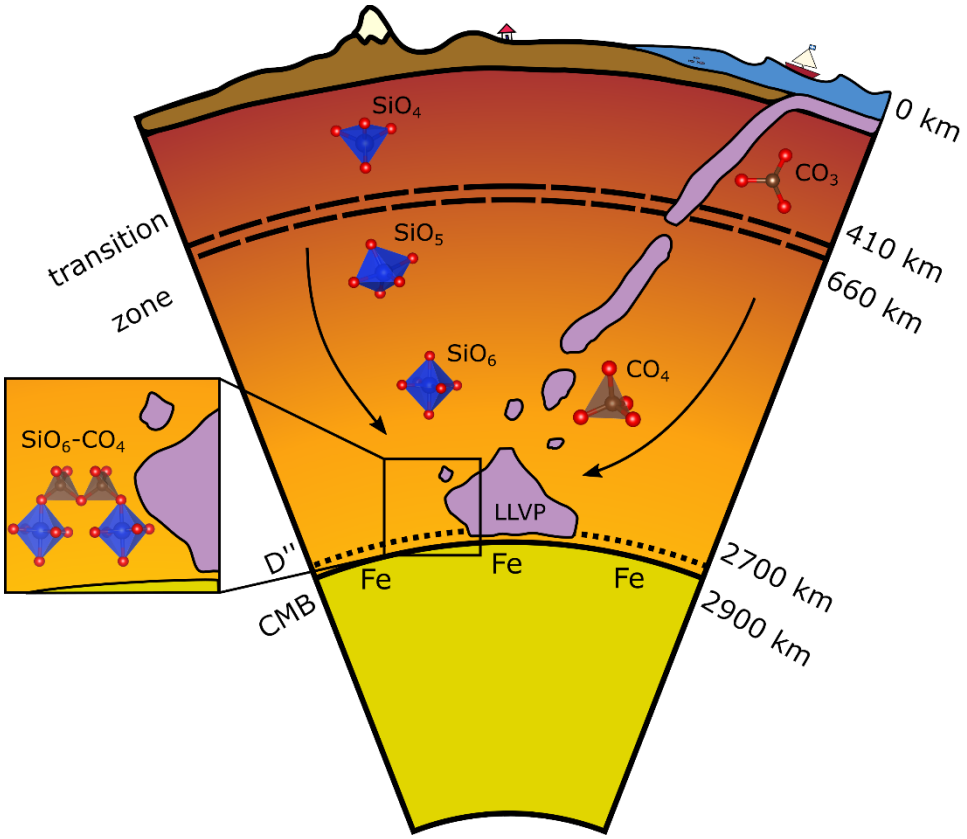


Figure 4. Schematic diagram of a possible silicate-carbonate formation path in the mantle. Solid arrows indicate the coordination number increase with depth, from SiO_4 to SiO_6 in silicates and CO_3 to CO_4 in carbonates. The area close to the core-mantle boundary (CMB) where carbonate-rich subducted slabs, silicates from the surrounding mantle, and iron-rich material from the outer core interact, is a possible domain of silicate-carbonate formation.

Silicate-carbonate $CaSiC_2O_7$ was obtained as a product of the subsolidus reaction between $CaCO_3$ and $CaSiO_3$ in the presence of FeO at conditions close to the core-mantle boundary. Interestingly, all starting minerals have been proposed as possible components of the large low velocity provinces (LLVPs) (Dobson and Brodholt 2005; Marcondes 2016; Thomson et al. 2019; Cerantola et al. 2023; H. Wang et al. 2024; Zhou et al. 2025) that extend thousands of kilometres horizontally and hundreds of kilometres vertically on the core-mantle boundary and are seismologically detected below Africa and Pacific ocean (Li and Romanowicz 1996; Wen 2001; Romanowicz and Gung 2002). $CaSiC_2O_7$ being the first representative of the high-pressure silicate-carbonate class, it is of interest to examine its elastic properties and possible contribution of such group of compounds to the seismic signatures of the lowermost lower mantle. For this, the elastic moduli and acoustic wave velocities at 122 GPa were derived from the calculated elastic parameters (C_{ij}) as described in Texts S1 and S2. Their values are compared in Table 1 with the radial Reference Earth model (REM1D) (Moulik and Ekström 2025), with minerals of the pyrolitic lower mantle assemblage (Frost 2008) and with relevant high-pressure calcium carbonates. Interestingly, $CaSiC_2O_7$ is closer in elastic properties to carbonates rather than silicates and together they belong to the class of low-density minerals with low compressional and shear velocities (V_p and V_s respectively). This is in line with the observation on the bulk moduli of low-pressure silicate-carbonates, composed of CO_3 and SiO_4 units: there is negative correlation between CO_3 content and compressibility (Gao et al. 2015). Our results demonstrate that in the case of a reaction between silicates and carbonates within or at the boundaries of LLVPs, the possible formation of silicate-carbonates will reduce the bulk density (by consumption of dense $CaSiO_3$ and production of low-density carbon-bearing phases) and decrease the velocities. In addition, the particularly low shear modulus (188 GPa) of $CaSiC_2O_7$ indicates a shear-soft phase whose presence would facilitate plume formation. Deep-mantle plumes are associated with the edges of LLVPs where hotspots appear (Doucet et al. 2020; Koppers et al. 2021), emphasizing the potential importance of silicate-carbonates when formed at these boundaries.

The experimental confirmation of a silicate-carbonate phase suggests possible intricate chemical exchanges between carbonates and silicates in the heterogeneous lowermost mantle (Figure 4). Further systematic *in situ* investigations of carbon- and silicon- rich systems at across a range of pressures, temperatures and chemical compositions are lying ahead in order to clarify the potential role of silicate-carbonates in the mineralogy, geochemistry, and geophysics of Earth and Earth-like planets.

Table 1. Comparison of elastic properties of $CaSiC_2O_7$ with rock-forming minerals of the pyrolitic lower mantle and high-pressure carbonates at 122 GPa (~2700 km depth). The values derive from computational studies, except $Fe_{0.1}Mg_{0.9}O$ ferropericlase, where the values are extrapolated from the experimental data at lower-pressures.

	Compressional Wave Velocity / V_p (km/s)	Shear Wave velocity / V_s (km/s)	Density / ρ (g/cm^3)	Bulk Modulus / K (GPa)	Shear Modulus / G (GPa)	Reference
REM1D	13.57	7.21	5.47	627	284	(Moulik and Ekström 2025)
$CaSiC_2O_7$*	**12.45**	**6.01**	**5.198**	**555**	**188**	**this study**
CaC_2O_5*	13.24	6.98	5.05	560	245	(Wang et al. 2024)
post-aragonite $CaCO_3$*	13.34	7.22	5.29	571	275	(Marcondes 2016)
cubic $CaSiO_3$†	13.7	7.16	5.63	677	289	(Kawai and Tsuchiya 2015)
low-spin $Fe_{0.1}Mg_{0.9}O$‡§	13.1	6.97	5.6	600	271	(Marquardt et al. 2009)
Mg-perovskite‡	14.3	7.7	5.45	685	324	(Wan et al. 2024)
Mg-postperovskite‡	14.36	7.84	5.49	678	340	(Wentzcovitch et al. 2006)

*at 0 K.

†at 1000 K.

‡at 300 K.

§experimental data (extrapolated)

Methods

Sample preparation

A BX90 diamond anvil cell (DAC) equipped with synthetic diamond anvils with a culet size of 150 μm was prepared (Kantor et al. 2012). The rhenium gasket used was indented from an initial thickness of 220 μm down to 20 μm and laser-drilled to create a circular pressure chamber of 80 μm in diameter. A powdered natural sample of $CaSiO_3$ wollastonite containing small amounts of $CaCO_3$ (Figure S5) was loaded into the pressure chamber. A crystal of ^{57}Fe-enriched $Fe_{0.945}O$ of ~10 x 10 x 5 μm^3 (Kantor et al. 2008; Li et al. 2024) was also loaded to the pressure chamber, sandwiched by layers of $CaSiO_3$-$CaCO_3$ mixture at the top and at the bottom. The DAC was then compressed to 122(2) GPa as determined by the pressure-induced shift of the Raman spectrum of the diamonds at the culets (Akahama and Kawamura 2006). The sample was then heated for a few minutes from both sides at 2800(200) K using the double-sided Nd-YAG laser system at the Nuclear Resonance Beamline (ID18) (Kupenko et al. 2012, 2024; Aprilis et al. 2017) of the European Synchrotron Radiation Facility (ESRF) using the grey-body spectroradiometry method to measure the surface temperature of the heated sample (Heinz and Jeanloz 1987).

In situ single crystal X-Ray diffraction

In situ X-ray diffraction measurements were performed at the High-Pressure Diffraction Beamline ID15B (ESRF, Grenoble) (Garbarino et al. 2024). An EIGER2 X CdTe 9M detector was used and a monochromatic X-ray beam ($\lambda = 0.41505$ Å) was focused on the sample with a spot area of approximately 1.5 × 1.5 μm^2. An X-ray map of the laser-heated spot was obtained by scanning the sample chamber with a step of ~1.5 μm at $\omega = 0^o$. The resulting map was analysed using the XDI software suite (Hrubiak et al. 2019). At each position of interest, single-crystal datasets were collected during ω rotations of ±35° of the DAC with a step of 0.5°. The resulting diffraction images were analysed using the CrysAlisPro software suite. The Domain Auto Finder (DAFi) program was used to search for reflection groups belonging to the individual single crystal domains (Aslandukov et al. 2022). This approach allowed to identify several products of chemical reactions between $CaSiO_3$ and $CaCO_3$ in the presence of FeO, including the silicate-carbonate $CaSiC_2O_7$ described here. The crystal structure solution and refinement were performed using the Jana2006 software (Petříček et al. 2014). The Crystallographic Information File for $CaSiC_2O_7$ is deposited as Supporting Information as well as in the Cambridge Structural Database under deposition number CSD 2352267.

Computational Details.

The first-principles calculations were done using the framework of density functional theory (DFT) as implemented in the Vienna Ab initio Simulation Package (VASP) (Kresse and Furthmüller 1996). To expand the electronic wave function in plane waves we used the Projector-Augmented-Wave (PAW) method (Blöchl 1994; Kresse and Joubert 1999). The Generalized Gradient Approximation (GGA) functional was used for calculating the exchange-correlation energies, as proposed by Perdew–Burke–Ernzerhof (PBE) (Perdew et al. 1996). The PAW potentials with the following valence configurations of $3s^2 3p^6 4s^2$ for Ca ("Ca_sv"), $3s^2 3p^2$ for Si ("Si"), $2s^2 2p^2$ for C ("C") and $2s^2 2p^4$ for O ("O") were used. Convergence tests with a threshold of 2 meV per atom in energy led to a Monkhorst-Pack (Chadi 1977) *k*-point grid of 11x7x5 and an energy cut-off for the plane wave expansion of 750 eV. The phonon frequencies and phonon band structure calculations were performed in the harmonic approximation with non-analytical term correction with the help of PHONOPY software (Togo and Tanaka 2015) using the finite displacement method for 3x3x2 supercell (made for the primitive cell (PPOSCAR)) with respectively adjusted *k*-points: 4x4x2. Equation of state (EoS) calculations were performed via variable-cell structural relaxations between 1 bar and 160 GPa. In the static EoS calculations, the effect of zero-point motion and temperature was neglected. The elastic constants were obtained using the stress–strain method (Le Page and Saxe 2002).

Acknowledgements

We acknowledge the European Synchrotron Radiation Facility (ESRF) for provision of beamtime under proposal ES-1328 on the beamlines ID15B (High-Pressure Diffraction) and ID18 (Nuclear Resonance). The original data are stored at https://doi.esrf.fr/10.15151/ESRF-ES-1174622127 and https://doi.esrf.fr/10.15151/ESRF-ES-1106937230.

References

Agrosì, G., Tempesta, G., Mele, D., Caggiani, M.C., Mangone, A., Della Ventura, G., Cestelli-Guidi, M., Allegretta, I., Hutchison, M.T., Nimis, P., and others (2019) Multiphase inclusions associated with residual carbonate in a transition zone diamond from Juina (Brazil). Lithos, 350–351, 105279.

Akahama, Y., and Kawamura, H. (2006) Pressure calibration of diamond anvil Raman gauge to 310GPa. Journal of Applied Physics, 100, 043516.

Aprilis, G., Strohm, C., Kupenko, I., Linhardt, S., Laskin, A., Vasiukov, D.M., Cerantola, V., Koemets, E.G., McCammon, C., Kurnosov, A., and others (2017) Portable double-sided pulsed laser heating system for time-resolved geoscience and materials science applications. Review of Scientific Instruments, 88, 084501.

Arima, M., Kozai, Y., and Akaishi, M. (2002) Diamond nucleation and growth by reduction of carbonate melts under high-pressure and high-temperature conditions. Geology, 30, 691–694.

Aslandukov, A., Aslandukov, M., Dubrovinskaia, N., and Dubrovinsky, L. (2022) Domain Auto Finder (DAFi) program: the analysis of single-crystal X-ray diffraction data from polycrystalline samples. Journal of Applied Crystallography, 55, 1383–1391.

Bhatnagar, A., and Sillanpää, M. (2010) Utilization of agro-industrial and municipal waste materials as potential adsorbents for water treatment—A review. Chemical Engineering Journal, 157, 277–296.

Biellmann, C., Gillet, P., Guyot, F., Peyronneau, J., and Reynard, B. (1993) Experimental evidence for carbonate stability in the Earth's lower mantle. Earth and Planetary Science Letters, 118, 31–41.

Binck, J., Laniel, D., Bayarjargal, L., Khandarkhaeva, S., Fedotenko, T., Aslandukov, A., Glazyrin, K., Milman, V., Chariton, S., Prakapenka, V.B., and others (2022) Synthesis of calcium orthocarbonate, Ca2CO4-Pnma at P-T conditions of Earth's transition zone and lower mantle. American Mineralogist, 107, 336–342.

Blöchl, P.E. (1994) Projector augmented-wave method. Physical Review B, 50, 17953–17979.

Boulard, E., Gloter, A., Corgne, A., Antonangeli, D., Auzende, A.-L., Perrillat, J.-P., Guyot, F., and Fiquet, G. (2011) New host for carbon in the deep Earth. Proceedings of the National Academy of Sciences, 108, 5184–5187.

Boulard, E., Pan, D., Galli, G., Liu, Z., and Mao, W.L. (2015) Tetrahedrally coordinated carbonates in Earth's lower mantle. Nature Communications, 6, 6311.

Cerantola, V., Bykova, E., Kupenko, I., Merlini, M., Ismailova, L., McCammon, C., Bykov, M., Chumakov, A.I., Petitgirard, S., Kantor, I., and others (2017) Stability of iron-bearing carbonates in the deep Earth's interior. Nature Communications, 8, 15960.

Cerantola, V., Sahle, C.J., Petitgirard, S., Wu, M., Checchia, S., Weis, C., Di Michiel, M., Vaughan, G.B.M., Collings, I.E., Arató, R., and others (2023) Tetracarbonates in silicate melts may be at the origin of a deep carbon reservoir in the deep Earth. Communications Earth & Environment, 4, 67.

372 Chadi, D.J. (1977) Special points for Brillouin-zone integrations. Physical Review B, 16, 1746–1747.

373 Chariton, S. (2020) The elastic properties and the crystal chemistry of carbonates in the deep Earth.
374 Doctoral thesis, Bayreuth.

375 Chariton, S., Bykov, M., Bykova, E., Koemets, E., Fedotenko, T., Winkler, B., Hanfland, M.,
376 Prakapenka, V.B., Greenberg, E., McCammon, C., and others (2020) The crystal structures of
377 Fe-bearing MgCO3 sp 2- and sp 3-carbonates at 98 GPa from single-crystal X-ray diffraction
378 using synchrotron radiation. Acta Crystallographica. Section E, Crystallographic
379 Communications, 76, 715–719.

380 Dasgupta, R., and Hirschmann, M.M. (2010) The deep carbon cycle and melting in Earth's interior.
381 Earth and Planetary Science Letters, 298, 1–13.

382 Davis, A.H., Chidester, B.A., Greenberg, E., Prakapenka, V.B., and Campbell, A.J. (2024) Carbonate-
383 Metal Reactions in the Lower Mantle. ACS Earth and Space Chemistry, 8, 654–664.

384 Dobson, D.P., and Brodholt, J.P. (2005) Subducted banded iron formations as a source of ultralow-
385 velocity zones at the core–mantle boundary. Nature, 434, 371–374.

386 Dorfman, S.M., Badro, J., Nabiei, F., Prakapenka, V.B., Cantoni, M., and Gillet, P. (2018) Carbonate
387 stability in the reduced lower mantle. Earth and Planetary Science Letters, 489, 84–91.

388 Doucet, L.S., Li, Z.-X., Gamal El Dien, H., Pourteau, A., Murphy, J.B., Collins, W.J., Mattielli, N.,
389 Olierook, H.K.H., Spencer, C.J., and Mitchell, R.N. (2020) Distinct formation history for deep-
390 mantle domains reflected in geochemical differences. Nature Geoscience, 13, 511–515.

391 Drewitt, J.W.E., Walter, M.J., Zhang, H., McMahon, S.C., Edwards, D., Heinen, B.J., Lord, O.T.,
392 Anzellini, S., and Kleppe, A.K. (2019) The fate of carbonate in oceanic crust subducted into
393 earth's lower mantle. Earth and Planetary Science Letters, 511, 213–222.

394 Finkelstein, G.J., Dera, P.K., and Duffy, T.S. (2015) Phase transitions in orthopyroxene (En90) to 49
395 GPa from single-crystal X-ray diffraction. Physics of the Earth and Planetary Interiors, 244,
396 78–86.

397 Fleet, M.E., and Henderson, G.S. (1995) Sodium trisilicate: A new high-pressure silicate structure
398 (Na2Si[Si2O7]). Physics and Chemistry of Minerals, 22, 383–386.

399 Frost, D. j, Mann, U., Asahara, Y., and Rubie, D. c (2008) The redox state of the mantle during and
400 just after core formation. Philosophical Transactions of the Royal Society A: Mathematical,
401 Physical and Engineering Sciences, 366, 4315–4337.

402 Frost, D.J. (2008) The Upper Mantle and Transition Zone. Elements, 4, 171–176.

403 Frost, D.J., and McCammon, C.A. (2008) The Redox State of Earth's Mantle. Annual Review of Earth
404 and Planetary Sciences, 36, 389–420.

405 Frost, D.J., and Myhill, R. (2016) Chemistry of the Lower Mantle. In Deep Earth pp. 225–240.
406 American Geophysical Union (AGU).

407 Frost, D.J., Liebske, C., Langenhorst, F., McCammon, C.A., Trønnes, R.G., and Rubie, D.C. (2004)
408 Experimental evidence for the existence of iron-rich metal in the Earth's lower mantle.
409 Nature, 428, 409–412.

Gao, J., Wu, X., and Qin, S. (2015) The crystal chemistry and the compressibility of silicate-carbonate minerals: Spurrite, galuskinite and tilleyite. Geoscience Frontiers, 6, 771–777.

Gao, J., Wu, X., Yuan, X., and Su, W. (2022) Fate of Carbonates in the Earth's Mantle (10-136 GPa). Frontiers in Earth Science, 10.

Garbarino, G., Hanfland, M.E., Gallego-Parra, S., Rosa, A.D., Mezouar, M., Duran, D., Martel, K., Papillon, E., Roth, T., Got, P., and others (2024) Extreme conditions X-ray diffraction and imaging beamline ID15B on the ESRF extremely brilliant source. High Pressure Research, 44, 199–216.

Grice, J.D. (2005) THE STRUCTURE OF SPURRITE, TILLEYITE AND SCAWTITE, AND RELATIONSHIPS TO OTHER SILICATE–CARBONATE MINERALS. The Canadian Mineralogist, 43, 1489–1500.

Grochala, W., Hoffmann, R., Feng, J., and Ashcroft, N.W. (2007) The Chemical Imagination at Work in Very Tight Places. Angewandte Chemie International Edition, 46, 3620–3642.

Gu, T., Li, M., McCammon, C., and Lee, K.K.M. (2016) Redox-induced lower mantle density contrast and effect on mantle structure and primitive oxygen. Nature Geoscience, 9, 723–727.

Hazen, R.M., Downs, R.T., and Finger, L.W. (1996) High-Pressure Framework Silicates. Science, 272, 1769–1771.

Hazen, R.M., Downs, R.T., and Prewitt, C.T. (2018) 1. Principles of Comparative Crystal Chemistry. In 1. Principles of Comparative Crystal Chemistry pp. 1–34. De Gruyter.

Heinz, D.L., and Jeanloz, R. (1987) Temperature Measurements in the Laser-Heated Diamond Cell. In High-Pressure Research in Mineral Physics: A Volume in Honor of Syun-iti Akimoto pp. 113–127. American Geophysical Union (AGU).

Hirschmann, M.M. (2023) The deep Earth oxygen cycle: Mass balance considerations on the origin and evolution of mantle and surface oxidative reservoirs. Earth and Planetary Science Letters, 619, 118311.

Hrubiak, R., Smith, J.S., and Shen, G. (2019) Multimode scanning X-ray diffraction microscopy for diamond anvil cell experiments. Review of Scientific Instruments, 90, 025109.

Hu, Y., Kiefer, B., Bina, C.R., Zhang, D., and Dera, P.K. (2017) High-Pressure γ-$CaMgSi_2O_6$: Does Penta-Coordinated Silicon Exist in the Earth's Mantle? Geophysical Research Letters, 44, 11,340-11,348.

Kakizawa, S., Inoue, T., Suenami, H., and Kikegawa, T. (2015) Decarbonation and melting in MgCO3–SiO2 system at high temperature and high pressure. Journal of Mineralogical and Petrological Sciences, 110, 179–188.

Kaminsky, F. (2012) Mineralogy of the lower mantle: A review of 'super-deep' mineral inclusions in diamond. Earth-Science Reviews, 110, 127–147.

Kaminsky, F.V. (2020) Basic problems concerning the composition of the Earth's lower mantle. Lithos, 364–365, 105515.

Kantor, I., Kurnosov, A., McCammon, C., and Dubrovinsky, L. (2008) Monoclinic FeO at high pressures. Zeitschrift für Kristallographie - Crystalline Materials, 223, 461–464.

448 Kantor, I., Prakapenka, V., Kantor, A., Dera, P., Kurnosov, A., Sinogeikin, S., Dubrovinskaia, N., and
449 Dubrovinsky, L. (2012) BX90: A new diamond anvil cell design for X-ray diffraction and
450 optical measurements. Review of Scientific Instruments, 83, 125102.

451 Kawai, K., and Tsuchiya, T. (2015) Small shear modulus of cubic CaSiO3 perovskite. Geophysical
452 Research Letters, 42, 2718–2726.

453 König, J., Spahr, D., Bayarjargal, L., Gavryushkin, P.N., Sagatova, D., Sagatov, N., Milman, V.,
454 Liermann, H.-P., and Winkler, B. (2022) Novel Calcium sp3 Carbonate CaC2O5-I42d May Be a
455 Carbon Host in Earth's Lower Mantle. ACS Earth and Space Chemistry, 6, 73–80.

456 Koppers, A.A.P., Becker, T.W., Jackson, M.G., Konrad, K., Müller, R.D., Romanowicz, B., Steinberger,
457 B., and Whittaker, J.M. (2021) Mantle plumes and their role in Earth processes. Nature
458 Reviews Earth & Environment, 2, 382–401.

459 Korsakov, A.V., and Hermann, J. (2006) Silicate and carbonate melt inclusions associated with
460 diamonds in deeply subducted carbonate rocks. Earth and Planetary Science Letters, 241,
461 104–118.

462 Kovalev, V., Spahr, D., Winkler, B., Bayarjargal, L., Wedek, L., Aslandukova, A., Pakhomova, A.,
463 Garbarino, G., and Bykova, E. (2025) High-pressure synthesis and crystal structure of iron
464 sp3-carbonate (Fe2[C4O10]) featuring pyramidal [C4O10]4- anions. Communications
465 Chemistry, 8, 1–11.

466 Kresse, G., and Furthmüller, J. (1996) Efficient iterative schemes for ab initio total-energy
467 calculations using a plane-wave basis set. Physical Review B, 54, 11169–11186.

468 Kresse, G., and Joubert, D. (1999) From ultrasoft pseudopotentials to the projector augmented-wave
469 method. Physical Review B, 59, 1758–1775.

470 Krivovichev, S.V. (2021) High-pressure Silicates: Crystal Chemistry and Systematics. Zapiski Rmo
471 (proceedings of the Russian Mineralogical Society), 150, 1–78.

472 Kunther, W., Ferreiro, S., and Skibsted, J. (2017) Influence of the Ca/Si ratio on the compressive
473 strength of cementitious calcium–silicate–hydrate binders. Journal of Materials Chemistry A,
474 5, 17401–17412.

475 Kupenko, I., Dubrovinsky, L., Dubrovinskaia, N., McCammon, C., Glazyrin, K., Bykova, E., Ballaran,
476 T.B., Sinmyo, R., Chumakov, A.I., Potapkin, V., and others (2012) Portable double-sided laser-
477 heating system for Mössbauer spectroscopy and X-ray diffraction experiments at
478 synchrotron facilities with diamond anvil cells. Review of Scientific Instruments, 83, 124501.

479 Kupenko, I., Li, X., Müller, S.C., Bessas, D., Yaroslavtsev, S., Aprilis, G., Chumakov, A.I., Celse, J.-P., and
480 Rüffer, R. (2024) Nuclear resonance techniques for high-pressure research: example of the
481 ID18 beamline of the European Synchrotron Radiation Facility. High Pressure Research, 44,
482 310–336.

483 Larsen, E.S., and Dunham, K.C. (1933) Tilleyite, a new mineral from the contact zone at Crestmore,
484 California. American Mineralogist, 18, 469–473.

485 Lazic, B., Armbruster, T., Savelyeva, V.B., Zadov, A.E., Pertsev, N.N., and Dzierżanowski, P. (2011)
486 Galuskinite, Ca7(SiO4)3(CO3), a new skarn mineral from the Birkhin gabbro massif, Eastern
487 Siberia, Russia. Mineralogical Magazine, 75, 2631–2648.

Le Page, Y., and Saxe, P. (2002) Symmetry-general least-squares extraction of elastic data for strained materials from ab initio calculations of stress. Physical Review B, 65, 104104.

Lebedev, S., Chevrot, S., and van der Hilst, R.D. (2002) Seismic Evidence for Olivine Phase Changes at the 410- and 660-Kilometer Discontinuities. Science, 296, 1300–1302.

Li, X., Bykova, E., Vasiukov, D., Aprilis, G., Chariton, S., Cerantola, V., Bykov, M., Müller, S., Pakhomova, A., Akbar, F.I., and others (2024) Monoclinic distortion and magnetic transitions in FeO under pressure and temperature. Communications Physics, 7, 1–11.

Li, X.-D., and Romanowicz, B. (1996) Global mantle shear velocity model developed using nonlinear asymptotic coupling theory. Journal of Geophysical Research: Solid Earth, 101, 22245–22272.

Liu, L., and Lin, C.-C. (1995) High-pressure phase transformations of carbonates in the system CaoMgOSiO2CO2. Earth and Planetary Science Letters, 134, 297–305.

Lobanov, S.S., Dong, X., Martirosyan, N.S., Samtsevich, A.I., Stevanovic, V., Gavryushkin, P.N., Litasov, K.D., Greenberg, E., Prakapenka, V.B., Oganov, A.R., and others (2017) Raman spectroscopy and x-ray diffraction of ${\mathit{sp}}^{3}\phantom{\rule{4pt}{0ex}}\mathrm{CaC}{\mathrm{O}}_{3}$ at lower mantle pressures. Physical Review B, 96, 104101.

Lv, M., Dorfman, S.M., Badro, J., Borensztajn, S., Greenberg, E., and Prakapenka, V.B. (2021) Reversal of carbonate-silicate cation exchange in cold slabs in Earth's lower mantle. Nature Communications, 12, 1712.

Marcondes, M.L. (2016) Carbonates at high pressures: Possible carriers for deep carbon reservoirs in the Earth's lower mantle. Physical Review B, 94.

Marincea, Ş., Dumitraş, D.-G., Călin, N., Anason, A.M., Fransolet, A.M., and Hatert, F. (2013) SPURRITE, TILLEYITE AND ASSOCIATED MINERALS IN THE EXOSKARN ZONE FROM CORNET HILL (METALIFERI MASSIF, APUSENI MOUNTAINS, ROMANIA). The Canadian Mineralogist, 51, 359–375.

Marquardt, H., Speziale, S., Reichmann, H.J., Frost, D.J., and Schilling, F.R. (2009) Single-crystal elasticity of (Mg0.9Fe0.1)O to 81 GPa. Earth and Planetary Science Letters, 287, 345–352.

Merlini, M., Hanfland, M., Salamat, A., Petitgirard, S., and Müller, H. (2015) The crystal structures of Mg2Fe2C4O13, with tetrahedrally coordinated carbon, and Fe13O19, synthesized at deep mantle conditions. American Mineralogist, 100, 2001–2004.

Merlini, M., Cerantola, V., Gatta, G.D., Gemmi, M., Hanfland, M., Kupenko, I., Lotti, P., Müller, H., and Zhang, L. (2017) Dolomite-IV: Candidate structure for a carbonate in the Earth's lower mantle. American Mineralogist, 102, 1763–1766.

Merlini, M., Milani, S., and Maurice, J. (2020) Structures and Crystal Chemistry of Carbonate at Earth's Mantle Conditions. In Carbon in Earth's Interior pp. 87–95. American Geophysical Union (AGU).

Mouhat, F., and Coudert, F.-X. (2014) Necessary and sufficient elastic stability conditions in various crystal systems. Physical Review B, 90, 224104.

527 Moulik, P., and Ekström, G. (2025) Radial structure of the Earth: (II) Model features and
528 interpretations. Physics of the Earth and Planetary Interiors, 361, 107320.

529 Oganov, A.R., Ono, S., Ma, Y., Glass, C.W., and Garcia, A. (2008) Novel high-pressure structures of
530 MgCO3, CaCO3 and CO2 and their role in Earth's lower mantle. Earth and Planetary Science
531 Letters, 273, 38–47.

532 Oganov, A.R., Hemley, R.J., Hazen, R.M., and Jones, A.P. (2013) Structure, Bonding, and Mineralogy
533 of Carbon at Extreme Conditions. Reviews in Mineralogy and Geochemistry, 75, 47–77.

534 Ono, S., Kikegawa, T., and Ohishi, Y. (2007) High-pressure transition of CaCO3. American
535 Mineralogist, 92, 1246–1249.

536 Pakhomova, A., Bykova, E., Bykov, M., Glazyrin, K., Gasharova, B., Liermann, H.-P., Mezouar, M.,
537 Gorelova, L., Krivovichev, S., and Dubrovinsky, L. (2017) A closer look into close packing:
538 pentacoordinated silicon in a high-pressure polymorph of danburite. IUCrJ, 4, 671–677.

539 Pakhomova, A., Simonova, D., Koemets, I., Koemets, E., Aprilis, G., Bykov, M., Gorelova, L.,
540 Fedotenko, T., Prakapenka, V., and Dubrovinsky, L. (2020) Polymorphism of feldspars above
541 10 GPa. Nature Communications, 11, 2721.

542 Pantousas, A., Aprilis, G., Aslandukova, A., Kupenko, I., Li, X., Zhou, W., Leveque, P., Hanfland, M.,
543 Dubrovinsky, L., and Pakhomova, A. (2025, October 31) Tetrahedral Frameworks and Helical
544 Chains: oP32– CaC2O5 and mP80– CaCO3 Calcium Carbonates above 100 GPa. Research
545 Square.

546 Penman, D.E., Caves Rugenstein, J.K., Ibarra, D.E., and Winnick, M.J. (2020) Silicate weathering as a
547 feedback and forcing in Earth's climate and carbon cycle. Earth-Science Reviews, 209,
548 103298.

549 Perdew, J.P., Burke, K., and Ernzerhof, M. (1996) Generalized Gradient Approximation Made Simple.
550 Physical Review Letters, 77, 3865–3868.

551 Petříček, V., Dušek, M., and Palatinus, L. (2014) Crystallographic Computing System JANA2006:
552 General features. Zeitschrift für Kristallographie - Crystalline Materials, 229, 345–352.

553 Prewitt, C.T., and Downs, R.T. (1998) Chapter 9. High-pressure crystal chemistry. In R.J. Hemley, Ed.,
554 Ultrahigh Pressure Mineralogy pp. 283–318. De Gruyter, Berlin, Boston.

555 Reuss, A. (1929) Berechnung der Fließgrenze von Mischkristallen auf Grund der Plastizitätsbedingung
556 für Einkristalle . ZAMM - Journal of Applied Mathematics and Mechanics / Zeitschrift für
557 Angewandte Mathematik und Mechanik, 9, 49–58.

558 Rohrbach, A., and Schmidt, M.W. (2011) Redox freezing and melting in the Earth's deep mantle
559 resulting from carbon–iron redox coupling. Nature, 472, 209–212.

560 Romanowicz, B., and Gung, Y. (2002) Superplumes from the Core-Mantle Boundary to the
561 Lithosphere: Implications for Heat Flux. Science, 296, 513–516.

562 Santamaria-Perez, D., Ruiz-Fuertes, J., Marqueño, T., Pellicer-Porres, J., Chulia-Jordan, R., MacLeod,
563 S., and Popescu, C. (2018) Structural Behavior of Natural Silicate–Carbonate Spurrite
564 Mineral, Ca5(SiO4)2(CO3), under High-Pressure, High-Temperature Conditions. Inorganic
565 Chemistry, 57, 98–105.

566 Santamaria-Perez, D., Ruiz-Fuertes, J., Peña-Alvarez, M., Chulia-Jordan, R., Marqueño, T., Zimmer, D.,
567 Gutiérrez-Cano, V., MacLeod, S., Gregoryanz, E., Popescu, C., and others (2019) Post-tilleyite,
568 a dense calcium silicate-carbonate phase. Scientific Reports, 9, 7898.

569 Santoro, M., Gorelli, F., Haines, J., Cambon, O., Levelut, C., and Garbarino, G. (2011) Silicon
570 carbonate phase formed from carbon dioxide and silica under pressure. Proceedings of the
571 National Academy of Sciences, 108, 7689–7692.

572 Scrivener, K.L., John, V.M., and Gartner, E.M. (2018) Eco-efficient cements: Potential economically
573 viable solutions for a low-CO2 cement-based materials industry. Cement and Concrete
574 Research, 114, 2–26.

575 Seifu, M.N., Bersisa, A., Moon, K.-Y., Kim, G.M., Cho, J.-S., and Park, S. (2023) Exploring reaction and
576 carbonation products of calcium silicate cement. Journal of CO2 Utilization, 71, 102471.

577 Seto, Y., Hamane, D., Nagai, T., and Fujino, K. (2008) Fate of carbonates within oceanic plates
578 subducted to the lower mantle, and a possible mechanism of diamond formation. Physics
579 and Chemistry of Minerals, 35, 223–229.

580 Spahr, D., Binck, J., Bayarjargal, L., Luchitskaia, R., Morgenroth, W., Comboni, D., Milman, V., and
581 Winkler, B. (2021) Tetrahedrally Coordinated sp3-Hybridized Carbon in Sr2CO4
582 Orthocarbonate at Ambient Conditions. Inorganic Chemistry, 60, 5419–5422.

583 Thomson, A.R., Crichton, W.A., Brodholt, J.P., Wood, I.G., Siersch, N.C., Muir, J.M.R., Dobson, D.P.,
584 and Hunt, S.A. (2019) Seismic velocities of CaSiO3 perovskite can explain LLSVPs in Earth's
585 lower mantle. Nature, 572, 643–647.

586 Togo, A., and Tanaka, I. (2015) First principles phonon calculations in materials science. Scripta
587 Materialia, 108, 1–5.

588 Wan, T., Luo, C., Sun, Y., and Wentzcovitch, R.M. (2024) Thermoelastic properties of bridgmanite
589 using deep-potential molecular dynamics. Physical Review B, 109, 094101.

590 Wang, H., Liu, L., Gao, Z., Yang, L., Naren, G., and Mao, S. (2024) Structure and elasticity of CaC2O5
591 suggests carbonate contribution to the seismic anomalies of Earth's mantle. Nature
592 Communications, 15, 755.

593 Wang, Y., Bayarjargal, L., Bykova, E., Spahr, D., Bykov, M., Milman, V., Giordano, N., Fedotenko, T.,
594 Liermann, H.-P., and Winkler, B. (2024) Synthesis and Structure of Two New Cadmium
595 Carbonates at Extreme Conditions. Crystal Growth & Design, 24, 4143–4150.

596 Wen, L. (2001) Seismic evidence for a rapidly varying compositional anomaly at the base of the
597 Earth's mantle beneath the Indian Ocean. Earth and Planetary Science Letters, 194, 83–95.

598 Wentzcovitch, R.M., Tsuchiya, T., and Tsuchiya, J. (2006) MgSiO3 postperovskite at D" conditions.
599 Proceedings of the National Academy of Sciences, 103, 543–546.

600 Yang, J., Huang, J., Wang, H.-F., Wang, H., Yu, H., and Cao, Y. (2025) Preparation and modification of
601 carbon based materials as efficient catalysts in the cycloaddition of carbon dioxide towards
602 cyclic carbonates: a mini review. Catalysis Science & Technology, 15, 1771–1786.

603 Yao, X. (2018) Novel high-pressure calcium carbonates. Physical Review B, 98.

Zhang, P., Man, L., Yuan, L., Wu, X., and Zhang, J. (2025) Ultra-Low-Velocity Disordered CaCO3 May Explain Mid-Lithospheric Discontinuities. Journal of Geophysical Research: Solid Earth, 130, e2025JB031906.

Zhou, R. (2014) Unraveling Crystalline Structure of High-Pressure Phase of Silicon Carbonate. Physical Review X, 4.

Zhou, W.-Y., Hao, M., Su, W., Kim, T., Chen, S., Shim, S.-H., Zhang, D., Nguyen, P.Q.H., Armstrong, K., and Zhang, J.S. (2025) Elasticity of davemaoite as a primary contributor to lower-mantle heterogeneities. Science, 390, 935–939.

Zhu, F., Li, J., Liu, J., Lai, X., Chen, B., and Meng, Y. (2019) Kinetic Control on the Depth Distribution of Superdeep Diamonds. Geophysical Research Letters, 46, 1984–1992.

Supplementary Files

This is a list of supplementary files associated with this preprint. Click to download.

- C2CaO7Si.cif
- CaSiC2O7Supplementary.pdf
- CheckCIFCaSiC2O7.pdf